2. Stressed Ge:Ga Array

2.1 Design and Development Testing

Based on a paper by R. Schnurr, C. L. Thompson, J. T. Davis, J. W. Beeman, J. Cadien, E. T. Young, E. E. Haller, and G. H. Rieke in SPIE, 1998

2.1.1 Summary

The most suitable approach for detection of very low light levels in the 115 to 200μm range is Ge:Ga detectors stressed along the [100] crystal axis (Kazanskii, Richards, & Haller 1977; Haller, Hueschen, & Richards 1979). Stressed Ge:Ga has significant spaceflight heritage in the Long Wavelength Spectrometer (LWS) and ISOPHOT instruments for the Infrared Space Observatory (ISO) as well as the Far Infrared Line Mapper (FILM) on the Infrared Telescope in Space (IRTS). This detector type is the baseline for the 140 to 180μm channel of the Multiband Imaging Spectrometer for SIRTF (MIPS).

The goal for MIPS is to provide performance in the SIRTF orbit adequate to operate at the natural background limit due to thermal emission by zodiacal dust grains. For a typical quantum efficiency of 7% and responsivity of 7 A/W, a dark current less than 400e/s is required. The cosmic ray hit rate on the detectors is high, about 1/40sec in this orbit, requiring a low read noise of < 130 e rms to satisfy the sensitivity goal. To remove accumulated ionization damage from the cosmic ray hits, it must be possible to elevate the array temperature to re-thermalize the detector material, and this process must make minimal use of the liquid helium coolant. The array format is 2x20 pixels and the entire package must be small enough to fit within the compact packaging of the MIPS. If these requirements can be met, SIRTF will substantially outperform all previous missions in the very far infrared. We describe the array design that will provide this performance, along with some of the tests that confirm its behavior.

2.1.2. Design

2.1.2.1 Overall Concept

A stressing harness has been designed that allows a pixel-to-pixel spacing of 3mm in a 2x5 array format. This design is illustrated in Figure 2-1. The body of the stress rig is produced by electron discharge machining (EDM) from a single piece of Aermet 100 steel. This body includes the base, two leaf springs that are tapped at their ends for screws used to adjust the stress, and a central anvil against which the detector element is clamped. A separate Aermet 100 pressure distribution plate is placed between the tips of the stressing screws and the detector pixels.

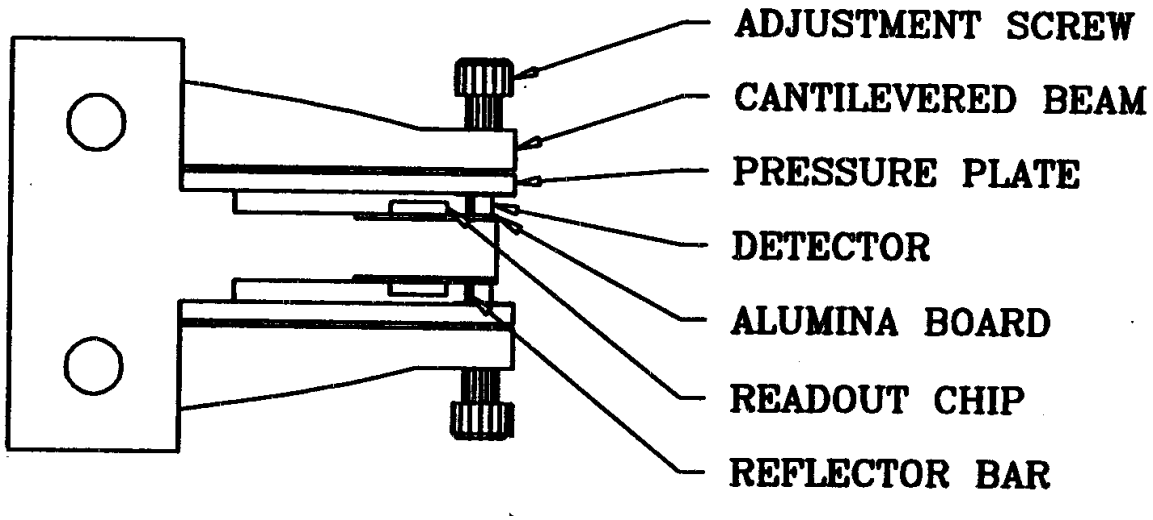

Figure 2-1. 2x5 Pixel Stressed Ge:Ga Detector Module. The cantilevered arm acts as a leaf spring and maintains a constant level of pressure on the detector. The pressure can be set with the adjustment screw, and the forces are controlled to be perpendicular to the detector face with the pressure plate. The readout integrated circuit, detector, and reflector bar portion of the integrating cavity around the detector are all mounted on an alumina board that is stressed within the module. This design minimizes the lead length between detector and readout, thus minimizing node capacitance on the readout and providing for small read noise.

An alumina circuit board, shown in Figure 2-2, lies against the anvil. Each board provides contacts for the five detectors on its side of the array. The pixels are stressed individually between the corresponding leaf spring and section of the anvil, through the pressure plate on one side and the alumina board on the other.

The leaf springs help to maintain an almost constant force on the pixels in the face of relaxation in the stressed stack. The leaf spring cross section has been designed to provide approximately uniform levels of stress along its length, while minimizing mass and allowing a reasonable adjustment range for the stressing screw (correct stress is obtained by bending the spring by about one screw turn). The spring is designed with a mechanical safety factor of 1.5 when the force is large enough to crush the detector. The pressure plate is as long as the leaf springs, but is much thinner. Its purpose is to avoid transmitting torque from the screw to the detector, but to be compliant in the stress direction so it does not affect the force being applied by the screw and spring. The anvil is made sufficiently thick that it deforms

only slightly under full stress, so that the failure of one pixel slightly reduces the stress on the pixel opposite but has little effect on the overall performance of the array.

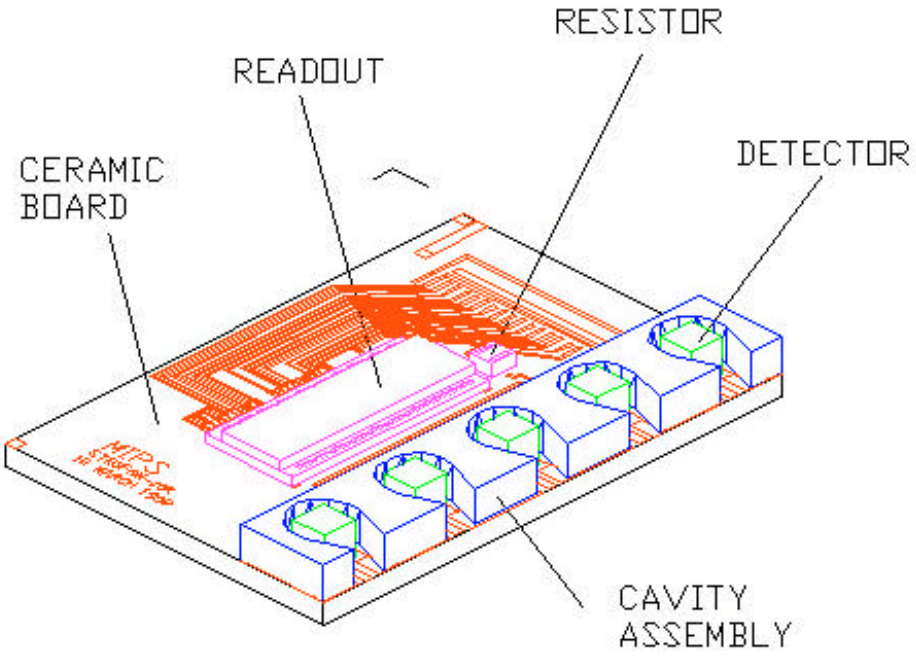

Figure 2-2. Alumina Board with readout, detectors, sense resistor, and integrating cavities.

The electronic readout is mounted on the alumina board, very close to the detector to minimize capacitance on the ntegrating node, thus making a low read noise possible. To carry signals, a flex cable is epoxied to the alumina board and connected to its traces by wire bonds. The flex cable is stabilized by clamps onto the side of the stress harness and is terminated with a nanoconnector. Its conductors are of constantin to help maintain thermal isolation of the stress module.

An integrating cavity is built up of metallized alumina plates around each detector. Photons are conveyed to each detector integrating cavity with a feedhorn also manufactured by EDM in Aermet 100 and attached with screws to the front of the stress harness. The feedhorns provide an array that is nearly filled optically despite the very low intrinsic fill factor of the array (1mm pixels on ~ 3mm centers). To provide a thick stressing anvil for a robust design, the completed module has two columns of five detectors separated by a space of one pixel width. We found that conventional Winston horns, which have a sharp cutoff in acceptance angle, were unsatisfactory for the feedhorns because the acceptance angle of the horns was too narrow to allow concentration of the energy diffracted at the horn entrance aperture.

Therefore, the feedhorns are designed to have a wide acceptance angle, ~ 6 degrees. The calculated transfer efficiency of the feedhorns is ~ 80%; that is, 80% of the photons that enter the 3mm feedhorn from the instrument optical train will be concentrated and emerge from the 0.7mm exit aperture into the detector integrating cavity.

The full 2 x 20 array will be built of four identical 2x5 pixel modules mounted on a thermal isolation and alignment structure as shown in Figure 2-3. The TIAS supports the backplane flex cable with connectors for the flex cables associated with each 2x5 pixel module. The backplane cable conducts signals to and from two MDM 51-pin connectors, one at each end of the TIAS. The array modules are attached to copper heat sinks that are mounted on thin

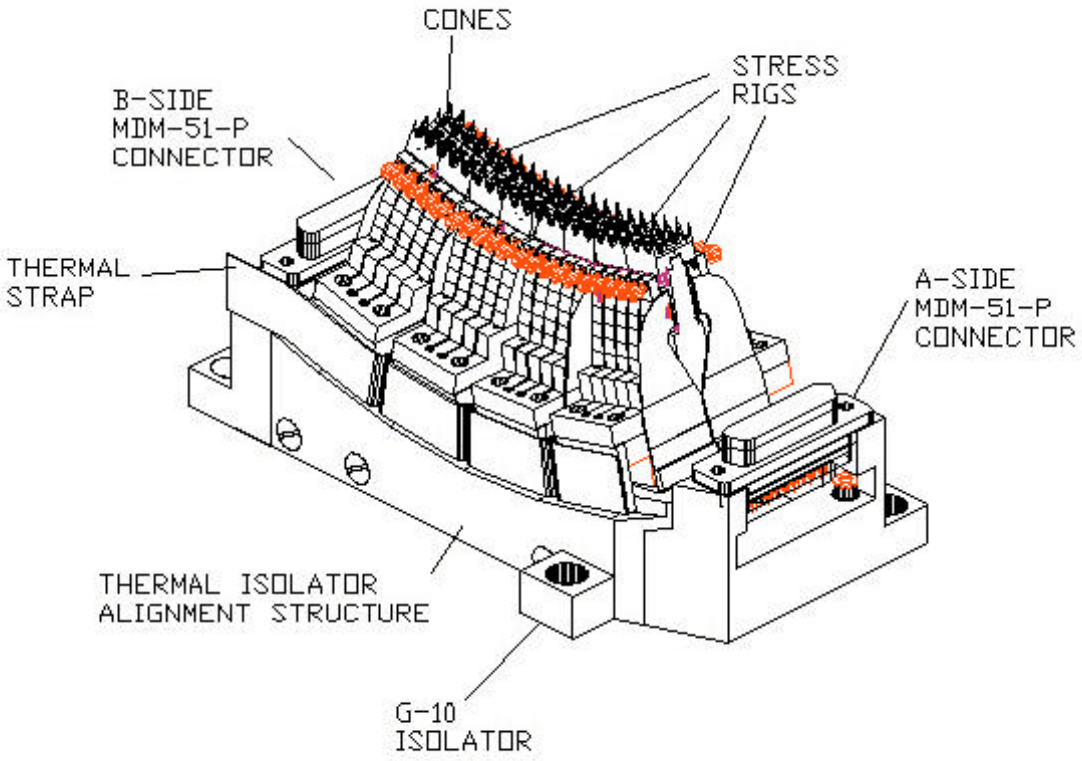

Figure 2-3. Full 2x20 Stressed Ge:Ga Array

wall G10 tubes to isolate them from the rest of the base (total conduction from all stress modules to the base will be < 2mW/K). A finite element analysis of the G10 mounts (by B. Snyder of Ball Aerospace) shows a safety factor of nearly three for the worst case combination of thermal and vibrational strain. The primary thermal path to the 1.4K SIRTF helium bath is through a copper thermal strap that will be attached with Stycast to the heat sinks. The thermal impedance of this strap will be dominated by the Stycast and can be controlled by adjusting the thickness and area of this joint.

The TIAS aims the 10 horns for each stress rig at a pupil formed by the instrument optical train. Because the feedhorns cannot be used for cold baffling of the detectors, cold baffles

are formed at another pupil early in the instrument optical train, and loose baffles are placed at the pupil viewed by the feedhorns to help suppress stray light within the instrument. The pupil viewed by the feedhorns is about 4mm in diameter and is formed at the surface of a small mirror. A small hole in the center of this mirror (~200μm in diameter) is the exit of an integrating cavity, one wall of which is a far infrared emission source used for calibration.

2.1.2.2. Thermal Performance

To allow a compact array that could be heated for thermal annealing required identification of an extremely strong material with low specific heat for the stress harness. To guide the search, a figure of merit was calculated based on the energy required to raise the temperature of the stressing leaf spring. This figure of merit combined the specific heat, volume, and yield strength of leaf springs designed of different materials. Among a variety of steels and BeCu, we found a good candidate in Aermet 100 steel, manufactured by Carpenter Technology. Aermet 100 is a Martensite steel, so it should not undergo a brittle transition at low temperatures. Limited information was available on its behavior at 77K and none at 4K, so we measured the low temperature properties of interest in our application.

Although Aermet 100 has very high fracture toughness at room temperature and 77K, to test it further we increased the stress in a prototype stressing harness to roughly twice the level required in our application (as measured by the bending of the leaf springs) and cooled it repeatedly to 2K. There was no damage.

The great strength of Aermet 100 was promising in terms of minimizing the volume, and hence the heat capacity, of the stressing harness. The specific heat is a second critical parameter. The heat capacity was measured for a prototype stress rig. This unit was mounted in a liquid helium dewar, thermally isolated from the cold surface except for a thin copper wire to provide a controlled thermal path. A heater was used to adjust the temperature of the prototype; the properties of the thermal link were determined from the steady-state temperatures as a function of heater power. With the thermal link as a given, the heat capacity was measured by turning on the heater and monitoring the heating and cooling curves that resulted. These curves were smoothed and their slopes measured to calculate the heat capacity as a function of temperature. The results are shown in Table 2-1.

Table 2-1. Specific Heat of Aermet 100

Temp. (K)	C_P (J/K kg)
2	0.35
2.2	0.37
3.0	0.48
4.0	0.58
5.0	0.68

The performance in annealing was determined by constructing a thermal model which allowed variation of the thermal link properties, input heat, and heating duration to determine whether the requirements could be met. The temperature of the focal plane after application of heater power can be calculated as follows. If P_1 is applied at time t = 0 to a thermally isolated element of heat capacity C tied to a heat sink at temperature T_0 by a thermal link of G, then the temperature of the element above T_0 is given by

$$T_1(t) = \frac{P_1}{G}\left[1 - e^{-Gt/C}\right], \qquad t \geq 0$$

We take the heat capacity from an analytic fit to the values in Table 2-1. The dependence of heat conductivity for Stycast goes approximately as T in the range of interest.

The equation for array temperature was solved numerically, taking the mass of the four modules together at the estimated value of 250g. Typical results are shown in Figure 2-4. Application of 300mW of heater power for 5 seconds and with G ~ 10 T mW/K provides a satisfactory solution to the goal to heat the array above 5K and to recover to operating temperature in less than 60 seconds. Laboratory experiments verify the assumption in this calculation that the heat transfers quickly from the heater through the Aermet 100 stress harness. These results indicate that annealing to 5K can be conducted every 30 minutes within a time-averaged power budget of 1mW.

There are additional constraints on the thermal design. A value of G ~ 10 T mW/K limits the temperature rise of the array due to the power dissipation in the readouts to ~ 0.03K and allows the detectors to be cooled adequately for optimum performance. In addition, the branching ratio through this heat strap and the G10 standoffs for the array module heatsinks is low enough that instrument testing can be conducted with the optical bench only cooled with normal helium, a significant simplification in test requirements. Thermal modeling of the full instrument by C. Miller (Ball Aerospace) establishes that the detector pixels will be at ~ 1.7K if the detector heat sink is at 1.4K and the instrument optical bench is at 4.5K. At

1.7K, dark currents will be 1000 – 2000 e/s, too high to meet the sensitivity requirements for operation in space but adequately low for nearly all the instrument test program.

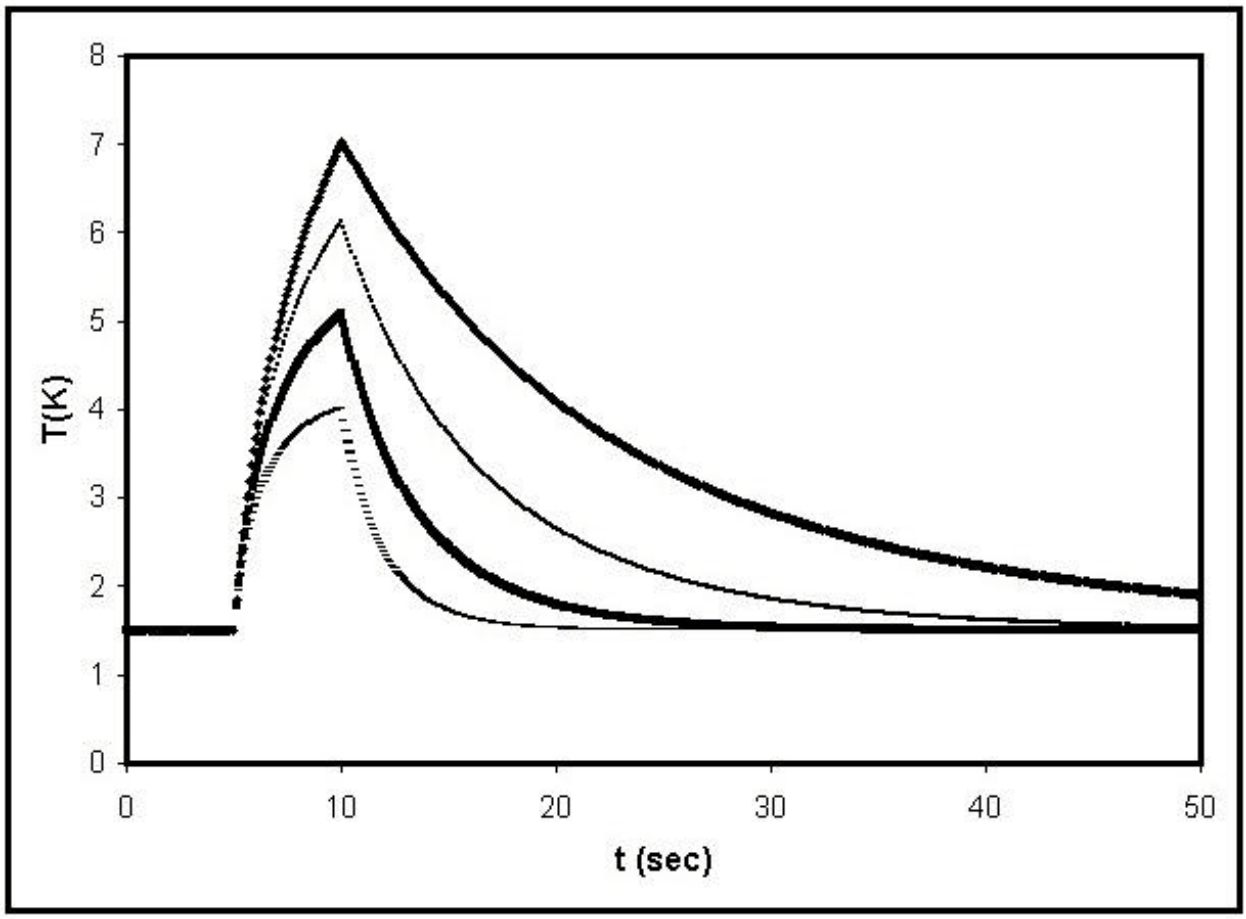

Figure 2-4. Behavior of Stressed Array During Annealing. All calculations are for application of heater power of 300mW for 5 seconds starting at a time of 5sec (with the array at 1.5K at that time). The thermal conductance to the heat sink is 2.5, 5, 10, and 20 times T mW/K respectively in order of decreasing peak temperature.

2.1.2.3. Readout

The readout for the detectors must satisfy a variety of requirements. Because the detectors operate at small bias, we use a CTIA circuit which stabilizes the bias through negative feedback to the input of the readout amplifier. The intrinsic read noise of the amplifier can be degraded by excess capacitance on its input node, which we have controlled by mounting the readout chip inside the jaws of the stressing harness and less than 1 cm from the detector pixels. However, when mounted in this position, the readout must operate at the detector temperature, ~ 1.5K. The charge carriers in conventional silicon integrated circuits freeze out at about 20K, which results in DC instabilities that would make the required level of bias stabiity impossible to maintain (as well as compromising the read noise).

The readouts we use were developed at Hughes Aircraft specifically to perform well in our application. They are grown on thin (~ 2.5 μm), low doped layers grown epitaxially on degenerately doped wafers. The heavily doped wafer maintains contact to the substrate even at out very low operating temperature, providing DC stability. A number of Hughes proprietary circuit design features also contribute to the low temperature performance. For further details regarding these CRC-696 readouts, see Young et al. (1995).

2.1.2.4. Array Circuit

Detector bias is established through the pressure plate. The other detector contact is accessed through a gold coated pad on the alumina board. A trace on the board goes from this pad underneath the wall of the integrating cavity to a bonding pad, and the connect on to the input of the readout is made by wire bonding from the bonding pad to an input pad of the readout. The readout is glued to the board with output and service lines all connected by wire bonding to traces delineated on the board. These traces lead to an array of pads at one edge of the board, which are wire bonded to pads on the flex cable, which provides the electrical interface to the external electronics.

A number of considerations led to this approach. First, it minimizes the distance between detector and amplifier, thus also minimizing the stray capacitance on the readout inputs, providing the lowest read noise. It also allows the entire mechanical and electrical aspects of a 5-pixel linear array to be constructed and tested for correct operation before committing the unit to the stress harness.

2.1.2.5. Detector Material

Detector material must be selected to provide good absorption and low dark current, requiring an optimization of the gallium concentration. Even with appropriate gallium concentrations, a high dark current is sometimes observed in the bulk material, associated in part with a high density of crystal dislocations. However, excellent performance has been demonstrated with a number of detector boules grown at Lawrence Berkeley National Laboratory (LBNL). For the MIPS arrays, we selected a region near the head end of Boule 113 that has a low threading dislocation density, less than 100 cm^{-3}. This boule has been extensively characterized because it is also used for the unstressed detector array being

constructed for MIPS. This crystal has a gallium concentration of 1.5 X 10^{14} cm^{-3}, with about 1% compensating donor impurities. The crystal was grown in the [100] direction, making it straightforward to cut wafers with the correct or entation for stressed Ge:Ga pixels.

2.1.3. Array Construction

2.1.3.1 Detector Preparation

In addition to bulk material properties, detector performance can be strongly influenced by the nature of the electrical contacts. Much of the non-photometric behavior reported for bulk photoconductors is attributed to large electric fields and their effects at imperfect contacts (Sclar 1984). Conduction due to surface damage from pixel processing can also dominate the dark current. Because of the above concerns, we prepare detector wafers as follows:

1.) 1.075 mm thick wafers are cut from the boule using a standard silicon technology saw.

2.) The flat surfaces of the wafer are hand lapped with 1900 grit SiC, and the wafer is cleaned with electronic grade methanol.

3.) The entire wafer is chemically etched for sixty seconds in a 7:2:1 mixture of HNO_3:HF:fuming HNO_3. This reduces the wafer to a final thickness of 1 mm. The etching is quenched with electronic grade methanol.

4.) Oxides are removed from the surfaces by soaking the wafer in a 1% HF (in water) solution for approximately three minutes.

5.) The flat surfaces are ion-implanted with boron in a two-step process:

1 X 10^{14} ions cm^{-2} @ 25 keV
2 X 10^{14} ions cm^{-2} @ 50 keV.

6.) The wafer is metallized with 0.02 microns Pd and then 0.4 microns Au by argon sputtering. It is then annealed for one hour at 300^{o}C in an inert gas atmosphere to remove any residual strain in the metallic layers and to activate the implanted boron layer.

Once a wafer is processed in this fashion, we can produce pieces of it that can be used as discrete detectors. The steps to do so are as follows:

1.) 1 mm^3.detector chips are cut from the wafer with a dicing saw. The blade of the saw is impregnated with 3 to 7 micron diamond grit, which produces a straight cut and leaves a minimum of surface damage on the cut edges. The detector chips are then cleaned with trichloroethane and methanol, and blown dry with nitrogen gas.

2.) The chips are etched for sixty seconds in the 7:2:1 etch solution and quenched in electronic grade methanol. The gold layer on the implanted electrodes masks the effect of the etch on the implanted surfaces, thereby protecting the contacts. The etch time is twice that required to remove surface damage, but we have found that the more rounded detector edges that result are resistant to chipping in the stress harness.

3.) Finally, the detectors are blown dry with nitrogen gas. They are then ready for mounting in the stressing harness. The final dimensions for the detectors are ~ 1 X 0.8 X 0.8 mm, with 1 mm between electrodes.

2.1.3.2. Assembly

The alumina board, readout, flex cable, and interconnects are built and tested as a unit prior to committing them to an array. Construction begins with photolithography on a metallized piece of alumina. After traces have been delineated, the alumina is diced into individual boards. The readout and flex cable are attached with epoxy to the alumina and the necessary wire bonds are made to pads on the board. The unit is tested for electrical aliveness. Next, individual integrating cavities for the detectors are built up by epoxying small pieces of metallized alumina to the board. Finally, a small piece of degenerately doped silicon (in practice, scrap readouts are used) is epoxied over the readout to keep its emissions from escaping and illuminating the detector. This complete unit is then tested again to determine readout performance and to verify that all the electrical connections have been established.

After it has been machined, the stress harness is prepared by polishing the anvil and the pressure plate surface that will contact the pixel. This step is critical to avoid breakage of pixels due to concentrated stress at surface irregularities. A completed alumina board that has passed the electrical performance screening is placed inside one side of the stress harness. Five detector pixels are loaded into a specially designed chuck that locates them precisely and simultaneously over the five pads on the alumina board. The chuck is inserted into the jaws of the harness, the pressure plate is tightened against the pixels, and the chuck is removed. The stress is then increased to the desired level by tightening the 1-72 screw threaded into the leaf spring. To avoid galling, the screw is lubricated with Molykote 321R. To keep the screw tip from wandering when it is tightened, it is rounded so it fits into a matching rounded depression in the pressure plate. To prevent lateral motion of the pressure plate, it is keyed into the rest of the stress harness.

The stress imposed on the detector can be measured by monitoring its room temperature resistance. The long wavelength extension of response saturates when the resistance has been brought down to 40% of its unstressed value. The extension of long wavelength response is only weakly dependent on level of stress at the prescribed level. Even with a room temperature resistance of 60% of the unstressed value, corresponding to 4000 kg cm^{-2}, full extension should be achieved within a few percent (Kazanskii, Richards, and Haller 1977). It has been demonstrated that the MIPS stress rig can provide enough force to reduce the pixel impedance to 20% of the unstressed value, a conf rmation that the forces are well controlled and uniform. The flight arrays will be stressed to 50%, allowing a substantial safety margin.

2.1.4 Performance

A full characterization of the infrared performance of the stressed array has not been completed, so we have estimated its behavior by a combination of tests on prototype SIRTF units plus individual detectors in a stress harness of different design.

2.1.4.1 Dark Current and Read Noise

Dark current and read noise are characteristic of the specific arrangement of components in the stressing harness, and hence have been measured in prototype MIPS devices. Initially, the design showed elevated dark current that exceeded the performance requirements by two orders of magnitude. Although it is not known whether this emission is thermal or nonthermal, the excess photons are concentrated at very long wavelengths: the dark current is only a few hundreds of e/s with minimal stress applied to a pixel (photoconductivity to ~ 120μm), but tens of thousands of e/s with stress to extend the response to 200μm. One possibility is that the signal arises from heating of small regions on the readout chip as current flows in the readout FETs. In any case, the dark current is suppressed by the degenerate silicon caps epoxied onto the tops of the readouts, which block the flow of photons from the surface of the chip. Of three 1x5 detector rows measured with this feature, the average dark current has been ~ 250 e/s (at 20mV bias and T = 1.4K).

Read noise is observed to be ~ 130 - 280 electrons rms. This value has been determined using "Lot 6" readouts, which are relatively noisy. "Lot 3" is the best lot of readouts we have, and is being reserved for the flight array build rather than being used in development of prototype units. The difference in read noise between these two lots is approximately a factor of two to three, so we expect to reach read noises of ~ 100 e rms in the flight units.

2.1.4.2. Responsivity, Quantum Efficiency

Most other array parameters should be, at least to first order, dependent on the detector material and hence can be estimated from tests in different stress harnesses so long as the level of stress is comparable.

Response measurements were conducted in a dewar with a divided internal dark chamber. A detector of the very similar Boule 773 material was mounted in one half of the chamber and could view through a small aperture an uncalibrated but very stable far infrared light source in the other half. This arrangement placed the prototype detector in virtually total dark with the infrared stimulator off and allowed study of the response at controlled levels of very faint illumination. The prototype detector was read out with a JF4 integrating JFET amplifier (manufactured by Infrared Laboratories, Inc.) with read noise of 40 electrons. To measure response, the stimulator was pulsed under computer control and readings with the stimulator off were subtracted from adjacent ones with it on.

The observed drop of about a factor of two in response between 2 K and 1.5 K suggests that the photoconductive gain may be reduced when the detector is conducting very low currents

(e.g., by dielectric relaxation). The observed change would correspond to a responsivity of 10 A/W at 1.5 K and 20 mV bias, normalized to measurements obtained with a high photon background where dielectric relaxation effects should have been minimal (i.e., 22 A/W at 163μm and 5 X 10^7 photons/sec). The reduction in response is roughly as predicted by the theory of Blouke et al. (1972). For our test, the dielectric time constant ranges from 1000 to 100,000 seconds, so all measurements are at frequencies far above the dielectric cutoff.

The detective quantum efficiency of the pixels is ~ 7%, in rough agreement with experience in other stress harnesses. It is unclear why this value is as low as it is, since the detector absorption is relatively high. There is evidence for excess noise associated with the placement of the detector pixels in some of these stress harnesses. The fact that the noise observed with the MIPS prototypes, using the Lot 6 readouts, is very similar to that observed with unstressed detectors and the same readouts, provides hope that the DQE of the flight devices will be higher than observed previously for other detector/readout arrangements.

2.1.4.3 Photometric Behavior

The detectors show two time constants in their response. The rapid component (to which the quoted responsivity refers) takes a fraction of a second and accounts for > 50% of the total. In addition, there is a slow response, time constant of tens of minutes, that is in accoradnce to first order with the predictions for dielectric relaxation. This slow response is an intrinsic behavior of bulk photoconductors, such as the stressed Ge:Ga detectors. It can substantially complicate calibration, since at low background it results in the observed signal level being a function of a long history of illumination on the detector. To circumvent these problems, MIPS includes a scan mirror that allows the signal to be modulated on and off the detectors at ~ 0.1 Hz, providing good separation of the "fast" signals from the "slow" ones.

The repeatability and the time dependence of the response of the prototype detector to extremely weak signals was measured by activating the stimulator in the helium cooled test chamber described in the preceding section. For these runs, the stimulator was set to give a signal of about 1000 electrons s^{-1}. Fifteen minutes of data were acquired in the dark, after which the stimulator was pulsed continuously for ten minutes with roughly 4 seconds on and 3 seconds off. Then the stimulator was left on for 15 minutes, after which data were again obtained for ten minutes with it pulsed. Average signals were computed over the ten minute intervals and compared as a function of the prior photon environment of the detector. The signals after soaking in illumination and in the dark are indistinguishable within the measurement accuracy. The deviations in signal strength around the average for all conditions are less $\pm$ 4% and generally fall within $\pm$ 2%. Therefore, so long as photometry can be obtained in the "fast" response regime for the detectors, it can be intrinsically accurate.

In operation in SIRTF, the photometric behavior will be complicated by the damage due to ionizing cosmic ray particles, which boosts the detector response. Tests with gamma radiation indicate that the detector NEP is not significantly degraded by this process until a significant dose has been accumulated, corresponding to a responsivity boost of nearly a

factor of two. Thus, annealing of the radiation damage will be required only every few hours. However, during the interim periods, the slow rise in response of the detector must be tracked and corrected to make use of its intrinsic ability to give photometric results. To provide frequent relative calibration, MIPS includes a stimulator near the entrance of the array feedhorns, so that calibration signals can be injected as frequently as is shown necessary by the in-orbit performance. The calibrator consists of a reverse bolometer stimulator that forms one wall of an integrating cavity. The exit aperture for the cavity is a small hole (~ 200μm in diameter) in the mirror placed at the pupil, and hence is in the center of the fields of all the detector feed horns. This geometry permits the stimulator to be flashed without disturbing the circumstances of measurement and hence gives a calibration of the "fast" response of the detector without exciting unnecessarily "slow" res onse activity.

2.1.4.4. Projected Performance in SIRTF

To estimate the performance of this array in SIRTF, we have assumed the following parameters:

Telescope Temperature	4.5K
Telescope Emissivity	30%
Pixel Size	λ/2.5D = 16"
Instrument Efficiency	50%
Detector Quantum Efficiency	7%
Responsivity	7 A/W
Read Noise	100 e rms

The performance in a ten second integration at the darkest regions of the sky is predicted to be a one standard deviation level of 0.5 mJy per pixel, or 4.3 mJy for a point source. The array becomes background limited in 3.4 seconds, so the signal to noise will improve with the square root of the integration time for longer observations. However, we expect SIRTF to become confusion limited on distant galaxies for integrations of 100 seconds and longer at 160μm (Rieke, Young, & Gautier 1995).

REFERENCES

1. A. G. Kazanskii, P. L. Richards, and E. E. Haller, "Far-Infrared Photoconductivity of Uni-Axially Stressed Germanium," App. Phys. Lett., 31, 496, 1977.
2. E. E. Haller, M. R. Hueschen, and P. L. Richards, "Ge:Ga Photoconductors in Low Infrared Backgrounds," App. Phys. Lett., 34, 495, 1979.
3. G. B. Heim, M. L. Henderson, K. MacFeely, T. J. McMahon, D. Michika, R. J. Pearson, G. H. Rieke, J. P. Schwenker, D. W. Strecker, C. Thompson, R. M. Warden, D. A. Wilson, and E. T. Young, "Multiband Imaging Photometer for SIRTF," SPIE Infrared Astronomical Instrumentation, paper 3354-07, March 1998

4. E. T. Young, G. H. Rieke, H. Dang, I. Barg, and C. L. Thompson, “Test Results for the SIRTF Far-Infrared Array Module,” SPIE Infrared Detectors and Instrumentation for Astronomy, 2475, 435, 1995
5. N. Sclar, “ Properties of Doped Silicon and Germanium Infrared Detectors,” Progress in Quantum Electronics, 9, 149, 1984.
6. M. M. Blouke, E. E. Harp, C. R. Jeffus, and R. L. Williams, “Gain Saturation in Extrinsic Germanium Photoconductors Operating at Low Temperature,” J. App. Phys., 43, 188, 1972.
7. G. H. Rieke, E. T. Young, and T. N. Gautier, “Detection Limits in the Far Infrared,” Space Sci. Rev. 74, 17, 1995